Encoding of Shape and Orientation of Objects Indented Into the Monkey Fingerpad by Populations of Slowly and Rapidly Adapting Mechanoreceptors

PARTAP S. KHALSA,[1] ROBERT M. FRIEDMAN,[1] MANDAYAM A. SRINIVASAN,[2] AND ROBERT H. LAMOTTE[1]

[1] *Department of Anesthesiology, Yale University School of Medicine, New Haven, Connecticut 06510; and* [2] *Research Lab of Electronics, Massachusetts Institute of Technology 36-796, Cambridge, Massachusetts 02139*

Khalsa, Partap S., Robert M. Friedman, Mandayam A. Srinivasan, and Robert H. LaMotte. Encoding of shape and orientation of objects indented into the monkey fingerpad by populations of slowly and rapidly adapting mechanoreceptors. *J. Neurophysiol.* 79: 3238–3251, 1998. The peripheral neural representation of object shape and orientation was studied by recording the responses of a spatially distributed population of rapidly and slowly adapting type I mechanoreceptors (RAs and SAs, respectively) to objects of different shapes and orientations indented at a fixed location on the fingerpad of the anesthetized monkey. The toroidal objects had a radius of 5 mm on the major axis, and 1, 3, or 5 mm on the minor axis. Each object was indented into the fingerpad for 4 s at orientations of 0, 45, 90, and 135° using a contact force of 15 gwt. Estimations of the population responses (PRs) were constructed by combining the responses of 91 SA and 97 RA single afferents at discrete times during the indentation. The PR was composed of the neural discharge rates (z coordinate) plotted at x and y coordinates of the most sensitive spot of the receptive field. The shapes of the PRs were related to the shapes of the objects by fitting the PRs with Gaussian surfaces. The orientations of the PRs were determined from weighted principal component analyses. The SA PR encoded both the orientation and shape of the objects, whereas the RA PR did neither. The SA PR orientation was biased toward the long axis of the finger. The RA PR encoded orientation only for the object with the highest curvature but did so ambiguously. Only the SA PR was well fit by a Gaussian surface. The shape of the object was discriminated by the SA PR within the first 500 ms of contact, and the form of the SA PR remained constant during the subsequent 3.5 s. This was manifested by constant widths of the PR along the major and minor axes despite a peak response that decreased from its maximum at 200 ms to an asymptotic value starting at 1 s. Thus the shape and orientation of each object were coded by the shape and orientation of the SA PR.

INTRODUCTION

Humans can readily perceive the shape and orientation of an object passively applied to the fingerpad (Goodwin et al. 1991; LaMotte et al. 1992; Wheat et al. 1995). The discrimination is maintained over a range of contact forces and areas (Goodwin and Wheat 1992a,b) and occurs whether the object is indented into or stroked across the finger (LaMotte and Srinivasan 1987; LaMotte et al. 1992; Srinivasan and LaMotte 1987).

The responses of single neurons cannot encode object shape and orientation because they can be confounded by the force and velocity of the applied stimulus (Burgess et al. 1983; Goodwin et al. 1991; Mei et al. 1983; Poulos et al. 1984). Further, some cutaneous mechanoreceptors exhibit directional sensitivity that, in principle, could alter their neural response even during indentation (Hulliger et al. 1979; Knibestol 1975; Srinivasan et al. 1990). Therefore, object shape and orientation must be encoded by a spatial population of mechanoreceptors (Cohen and Vierck 1993; Goodwin et al. 1995; LaMotte and Srinivasan 1996; LaMotte et al. 1996; Srinivasan and LaMotte 1991).

Simultaneously sampling the responses of an entire population of mechanosensitive afferents to a mechanical stimulus is currently beyond our technical ability. Previously, population responses were estimated from the responses of single neurons to an object indented at different locations with respect to the centers of their receptive fields. Afferent fibers were selected whose receptive fields were located centrally on a monkey fingerpad. Fixed aperiodic gratings (Philips and Johnson 1981), sinusoidally shaped steps (Srinivasan and LaMotte 1987), or spheres (Goodwin et al. 1995) were indented systematically at discrete distances from the center of the receptive fields while recording the response of the fiber. The responses were normalized and averaged to estimate how an actual population would respond to an indentation.

Interpreting the results from this approach of estimating a population response using a relatively sparse population has limitations. First, it is assumed that the skin of the fingerpad acts as a homogeneous and isotropic material that is flat. In reality, the skin is not only inhomogeneous and anisotropic but is also highly curved. This undoubtedly influences the responses of mechanoreceptors according to their locations. Second, when normalizing, it is assumed that mechanoreceptors respond in the same fashion. However, in reality, these afferents have different sensitivities and therefore exhibit different discharge rates. The CNS receives this nonnormalized information and, in some fashion, decodes the shape and orientation of an object. Hence, we decided to examine the population response to passive indentation without these limitations.

Previous indentation studies have focused either on the neural coding of two dimensional spatial forms (e.g., Phillips and Johnson 1981), step shapes (Srinivasan and LaMotte

0022-3077/98 $5.00

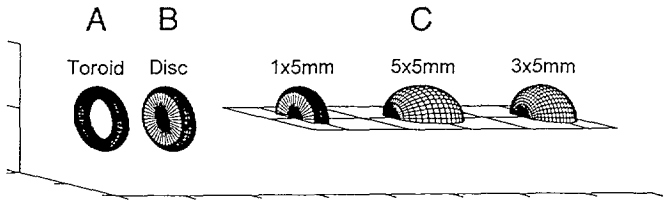

FIG. 1. Geometry of the objects used for indentation. *A*: toroid with a radius of 5 mm on its major axis and a radius of 1 mm on its minor axis. *B*: toroidal disk—a toroid the center of which has been filled with a flat cylinder. *C*: half toroidal disks the minor axis radii of which were 1, 3, and 5 mm. These 3 toroidal objects were mounted on a flat plate with their centers 18 mm apart. Tic mark spacing on each axis is 10 mm.

1987), cylinders (Srinivasan and LaMotte 1991), or three dimensional shapes of spheres (Goodwin et al. 1995). For indentation, there have been no studies on how the shapes and orientation of nonspherical, three-dimensional objects are independently coded in population responses of slowly and rapidly adapting, type I mechanoreceptors (SAs and RAs, respectively). Therefore the aim of the current study was to determine how a spatially representative population of cutaneous mechanoreceptors encoded the shape and orientation of toroidal and spherical objects during indentation.

METHODS

Three objects with smooth surfaces were milled from hard acrylic. Two were toroidally shaped and the other was spherical. The radii of the objects along the major axis were 5 mm (or a curvature of 200 m^{-1}), and 1, 3, and 5 mm (or curvatures of 1000, 333, and 200 m^{-1}, respectively) along the minor axis (Fig. 1). After cutting these objects so that their heights were 4 mm, they were mounted, with their long axes parallel, on a rectangular platform with their centers 18 mm apart (Fig. 1).

The hand of an anesthetized monkey was secured in a holder designed so that each digit could be repositioned reliably to the same angle during testing (Fig. 2). Digits were secured in individual supports by gluing a small peg onto the fingernail and locking the peg in a hole in the support. Each support could be raised up and locked into a fixed position at an angle of 25° from the horizontal. This angle presented the most sensitive and densely innervated portion of the fingerpad to the indenter.

The object platform was coupled via a force transducer (Brock Research, Natick, MA) to a force-controlled, torque motor (Model 305B, Cambridge Technologies, Watertown, MA; Fig. 2). The contact force normal to the skin was controlled by the torque motor and also was measured independently by the force transducer. The torque motor also measured angular displacement, which we calibrated into linear displacement. The torque motor was attached to a rotary platform which was attached to a three-axis, servo-controlled, brushless, linear actuator (Anorad, Hauppage, NY). The four-axis (x, y, z, and rotation, θ) programmable actuator (IDAC, Anorad) allowed positional control at the micrometer level, as well as precise control over velocity and acceleration for each axis. All data (x, y, z, θ positions, z displacement, Z force, and time of occurrence of discriminated action potentials) were collected at a rate of 1 kHz and stored directly to the hard disk of a laboratory computer for subsequent analysis.

The trajectory of the indentation followed a slight arc since it was controlled by the torque motor. To minimize in-plane forces (i.e., not normal to the skin) due to the trajectory, the object was aligned so that it would be normal to the skin during indentation on the fingerpad at an applied force of 15 gwt. Because the magnitudes of the indentations into the skin were small (~2–3 mm), it was determined that the actual compressional force was >99% of the recorded force.

Each object was indented into a fingerpad at the same relative x, y location (Fig. 2). The distal phalanges differ in geometry on a single hand and from monkey to monkey. To indent at the same relative y location (along the long axis of the finger), the object was centered one-third of the distance from the end of the phalange to the crease over the distal interphalangeal joint. This was done by first imaging the distal phalange from the side with a CCD camera equipped with a zoom lens. The magnified (about ×20) image was displayed on a monitor and its length measured. While viewing the image, the 1 × 5 mm object was precisely positioned along the y axis. The z axis (out of plane) was adjusted so that the object would be normal to the skin during indentation. Using a top-down, magnified view with a second camera, the object then was centered along the x axis.

Indentation protocol

Following the alignment procedure, each of the three objects was twice indented, from an initial position not touching the skin, on the fingerpad at four different orientations (0, 45, 90, and 135° relative to the x axis) using the following protocol. First, the 1 × 5 mm object was indented into the fingerpad for 4 s at a contact force of 15 gwt. The indentation occurred at a logarithmic rate with an approximately linear ramp of 66 gm/s during the first 100 ms and reached 67% (the 1st time constant) of the final 15 gwt in 200 ms (Fig. 3). There was no overshoot. For the first indentation, the major axis of the toroidal object was aligned with the

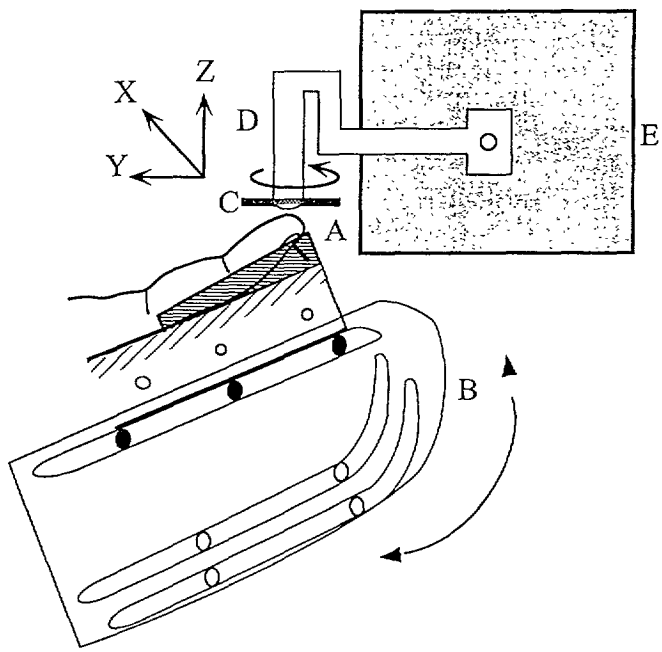

FIG. 2. Apparatus used for indenting the objects into the monkey fingerpad. Finger of the anesthetized monkey was secured in a contoured, acrylic finger mold (*A*) that was attached to a variable-angle finger holder (*B*). Platform (*C*) containing the 3 stimulus objects was attached to the 3-axis force transducer (*D*), mounted to a torque motor (E) that maintained the force applied to the object to the fingerpad. Torque motor was mounted on a rotary platform (not shown), which enabled rotation in the horizontal plane around the center of the fingerpad. Rotary platform was mounted to a 3-axis (w, y, z) translation table (not shown) that was used to align the objects above the fingerpad.

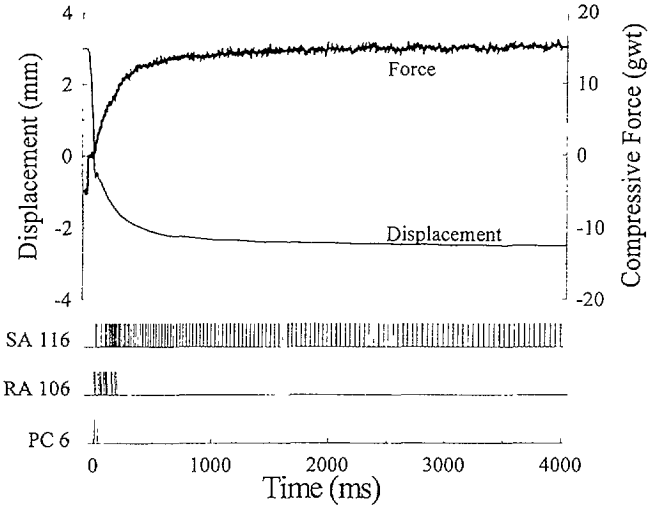

FIG. 3. Displacement and force during a typical indentation. Three raster plots are the times of ocurrences of action potentials for typical rapidly and slowly adapting type I mechanoreceptors (SA and RA, respectively) and rapidly adapting type II mechanoreceptor (PC).

long axis of the finger (i.e., the object was oriented at 90° in our finger coordinate system). After the 4 s of indentation, the object was stroked over the fingerpad in a specific paradigm for 15 s to acquire data for another experiment. The intertrial interval was 10 s between the end of the stroking paradigm and the next indentation. Second, the 1 × 5 mm object again was indented into the fingerpad at the same contact force and with the same orientation (90°) as the first indentation. After this indentation, a different stroking paradigm, but for the same length of time, was employed. For the third and fourth indentations, the object was rotated to 0° (major axis of the object aligned transverse to the long axis of the finger), and the two indentations and stroking paradigms previously described were repeated. The 5th–8th and the 9th–12th indentations were performed in the same sequence using the 3 × 5 and 5 × 5 mm objects, respectively. The same sequence of indentations using the three objects then was repeated for orientations of 45 and 135°.

The contact area of each of the three objects with the fingerpad was measured on one monkey using the following procedure. The left hand of the anesthetized monkey was secured in its hand/finger holder, and an object was aligned above the fingerpad as described previously. White, children's fingerpaint was applied to the surface of an object, and the object then was indented into the fingerpad for 4 s at a contact force of 15 gwt. The object then was lifted off the fingerpad and translated out of the field of view so that the white imprint of the contact region on the fingerpad could be imaged. This process was repeated for each of the three objects at orientations of 0° and 90° for digits 2, 3, and 4. The width, length, and area of the imaged contact regions for each of the indentations were subsequently measured using a commercial scanning package (SigmaScan Version 1.0, SPSS, Chicago, IL).

Discharges from single, mechanoreceptive neurons were recorded, using standard electrophysiological methods, from the median and ulnar nerves in anesthetized monkeys as has been previously described (LaMotte and Srinivasan 1987). Afferent fibers were recorded from the upper and lower portions of the nerves in adult (6–10 kg), male *Macaca mulatta* ($n = 4$) and *Macaca fascicularis* ($n = 1$). A monkey was sedated with ketamine hydrochloride (10 mg/kg im) and given atropine sulfate (0.04 mg/kg im). Surgical anesthesia was induced by isoflurane (2.0%) and a 60/40 mixture of nitrous oxide (N_2O) and oxygen (O_2). The animal was ventilated to maintain end-tidal carbon dioxide at 28 ± 2 (SE) mmHg and saturated O_2 at 100%. Pulse rate, blood pressures, and rectal temperature were monitored. Anesthesia was maintained by modulating the gas anesthetics to keep the pulse rate (100 ± 10 bpm) and blood pressures (100/50 ± 20/15 mmHg) within sufficient ranges to keep the animal areflexic to aversive stimuli. The temperature of the animal was maintained at 97 ± 2° by a heating pad enveloping the animal's torso and by covering the animal with a blanket. Hydration was maintained by a continuous drip of lactated Ringer solution (100 ml/h).

Receptor classification and receptive field mapping

After surgical exposure of the nerve, bundles of fibers were teased apart until the neural discharge of single neurons could be discriminated. Only low-threshold, mechanosensitive neurons (von Frey thresholds <5.1 gwt) innervating the glabrous skin of the distal phalanges (digits 2, 3, 4, or 5) were used. Afferents were classified as either slowly adapting type I (SA), rapidly adapting type I (RA), or rapidly adapting type II (Pacinian or PC) mechanoreceptors based on standard criteria. The receptive field of an identified mechanoreceptive fiber was mapped carefully using calibrated monofilaments (Stoelting. Chicago, IL). The most sensitive spot (MSS) (point with the lowest threshold to stimulation with a filament) was used as the planar location of the receptor ending on the finger.

Population response protocol

The response of a population of mechanoreceptors from the glabrous skin of a single distal phalange to indentation by the objects used in this study was constructed using the following protocol. The spatial location of the MSS for each mechanoreceptor was mapped from its actual coordinates to the analogous coordinates on a "virtual" or generic monkey finger. The geometry of the virtual finger was obtained from average values of *M. fascicularis* monkeys (Dandekar and Srinivasan 1995; Srinivasan 1989). Mapping was based on the position of the MSS relative to the center of indentation. The area encompassing the mapped units was 8.4 mm wide × 10.5 mm long, the average size of the monkey fingerpad. We attempted to isolate and record the neural responses from a large number of mechanoreceptors that were evenly distributed over this area.

Data analysis

The neural responses of an afferent to an indentation were binned using 100-ms intervals (0–100, 100–200, 200–300 ms, etc.) *Time 0* was defined as the occurrence of skin contact by the indenting object. This event was determined for each indentation by obtaining the second derivative of the indentation force and finding its characteristic peak that occurred when the object made contact with the skin. The estimated population responses (PRs) were constructed from the x, y coordinates of the location of the receptive fields MSS on the fingerpad and their discharge rates (impulses per 100 ms) representing the z coordinates. The PRs were represented as two-dimensional (2D) contour plots superimposed on geometric models of a virtual fingerpad, and as three-dimensional (3D) surface plots. Each of these methods of displaying the PR relied on a Kriging algorithm (Surfer, Version 6.02, Golden Software, Golden, CO). Essentially, Kriging is a statistical method of determining the best estimate for each point in a 3D matrix (Davis 1973). Missing data points are estimated using variance curves as weighting functions and a variance matrix is developed for the known and missing points. The "best" estimate is obtained by minimizing the values of the

variances. A strong feature of Kriging is that the values and locations of known data points are not altered.

Cross-sectional profiles were obtained through the centers of the PRs along the minor axes of the indenting objects to further examine how the widths and peaks of the PRs changed with curvature and time. The center profile for each PR was taken as the average of five profiles obtained at the center profile itself and ±0.25 mm and ±0.50 mm from the center profile. These distances were on the same order of magnitude as the average distances between the MSS of individual mechanoreceptors. The five profiles represented a width of 1 mm, which was approximately half of the contact width of the 1 × 5 mm object. Hence, these five profiles represented a common, approximate area of contact for the three objects.

The relationship between the PR and the shape of the object was examined by fitting the PR with an equation for a Gaussian surface of the form

$$z = f(x, y) = a \exp\{-0.5[(x - b/c)^2 + (y - d/e)^2]\}$$

with the x and y axes defined to be perpendicular and parallel respectively to the long axis of the finger. Although there are an infinite number of equations that could be fit to the PR, we chose to use a Gaussian surface equation for the following reasons. First, it is a general, nonlinear surface similar to that used by Goodwin et al. (1995) to fit population responses obtained from single fibers. Second, like our objects, it is symmetrical along a given axis, while allowing for differences in widths of the surface along orthogonal axes. Third, its parameters could be directly related to the geometry of the indenting objects. The parameters ($a - e$) of the equation all have direct physical interpretations as follows: a is the peak magnitude of the surface; b and d are the offsets of the surface from 0 for the x and y axes, respectively; and, c and e are the widths of the curves at 60.7% of the peak magnitude along the x and y axes, respectively. And, fourth, it is a robust equation to use when performing nonlinear regression. We employed a commercially available software (TableCurve 3D, SPSS), which allowed automated fitting of literally thousands of linear and nonlinear surface equations within a brief period of time. The surface fits were ranked by their adjusted coefficients of determination (adjusted R^2 values) and could be viewed selectively to observe the actual data plotted versus the surface fit. Thus we could compare empirically the fits of other surface equations to observe if another equation was consistently ranked higher than that of the simple Gaussian surface. The Gaussian surface equation is only suitable for data that are aligned with x and y axes. Hence, when the object was aligned at 45 or 135°, the data were first transformed by a coordinate rotation of 45 or 135° and then fit with the Gaussian equation.

Orientation

The orientation of the PR was determined by a weighted principal components analysis. The contribution of each mechanoreceptor was weighted by the number of action potentials that occurred during a selected 100-ms time period. This analysis produced two Eigenvectors (or principal components), each having a magnitude and angle (Morrison 1967). The orientation of the PR was determined by the angle of the first principal component. For each population, object, and 100-ms bin, an orientation was obtained; these data were plotted using polar coordinates (r = time and Φ = orientation angle). The mean orientations (with standard errors) of the PR over time to each object at a given orientation were obtained.

Horizontal extent of the PR

It was of interest to compare the area of a horizontal slice through the Gaussian fitted population response (PR_{Gf}) with that of the actual contact area of the object. Because the magnitude of a Gaussian surface only reaches zero at infinity, it was necessary to calculate the area of a slice through the "base" of the PR_{Gf} at a reasonable, though arbitrary, constraint on its magnitude. Accordingly, we evaluated the planar area of the PR_{Gf} to the 1 × 5 mm object oriented at 90° at two orders of magnitude (amplitude × 1/100) below the peak discharge. Areas for slices through all of the other PR_{Gf} were evaluated at this same value. Areas of these slices were calculated by the following procedure

Equation for a Gaussian surface centered at 0,0

$$z = a \exp\left\{-\frac{1}{2}\left[\left(\frac{x}{c}\right)^2 + \left(\frac{y}{e}\right)^2\right]\right\}$$

Solve equation for variable y

$$y = e\left[-2 \ln \frac{z}{a} - \left(\frac{x}{c}\right)^2\right]^{1/2}$$

Obtain area of slice by setting z to a particular value and integrating from $x$min to $x$max. The area is twice the integral because $y = f(x)$ is bivalued for each

$$\text{Area}_{\text{slice}} = 2\int_{x_{\min}}^{x_{\max}} e\left[-2 \ln \frac{z}{a} - \left(\frac{x}{c}\right)^2\right]^{1/2} dx$$

where a, c, and e are the same parameters as described previously (i.e., a = peak discharge, and c and e are the widths of the major and minor axis at 39.3% from the peak). Areas for each of the three PR_{Gf} at 90° were calculated using the respective values of the parameters (a, c, and e).

Statistics

Significance of the surface fit parameters was evaluated by one-way analyses of variance (ANOVAs) with repeated measures or Friedman's one-way ANOVAs (if the data failed a normality test) and pairwise comparisons between groups were done with the Student-Newman-Keuls method. Determination of the earliest time at which a discrimination could be made of the surface fit parameters was performed by a two-way ANOVA; pairwise comparisons were done with the Tukey method. The variance in the neural responses for the SA and RA populations due to different animals, left and right hands, and different fingers was evaluated for afferents stimulated by the 5 × 5 mm object, located within a 1.5 mm radius of the indentation site, and analyzed by one- and two-way ANOVAs as appropriate. All statistical tests were done with a probability criterion for significance of $\alpha = 0.05$.

RESULTS

The mechanoreceptor populations were constructed from the recordings of 91 SAs and 97 RAs from 20 experiments using five monkeys. The populations were distributed over an area of ~80 mm^2 giving a mean, approximate distribution of 1.1 SAs/mm^2 and 1.2 RAs/mm^2. Hence, our population densities were slightly smaller than those reported by Darian-Smith and Kennins (1980) of 1.3 SAs and 1.7 RAs per mm^2 but still provided a sufficiently large sample. Additionally, we recorded from six PCs. Four of the PCs were located on the digits and two on the palm. Ascertaining their precise receptive field locations was not possible, aside from two, which were localized to the distal phalanges. With rare exception, none of the afferents (SAs, RAs, and PCs) were

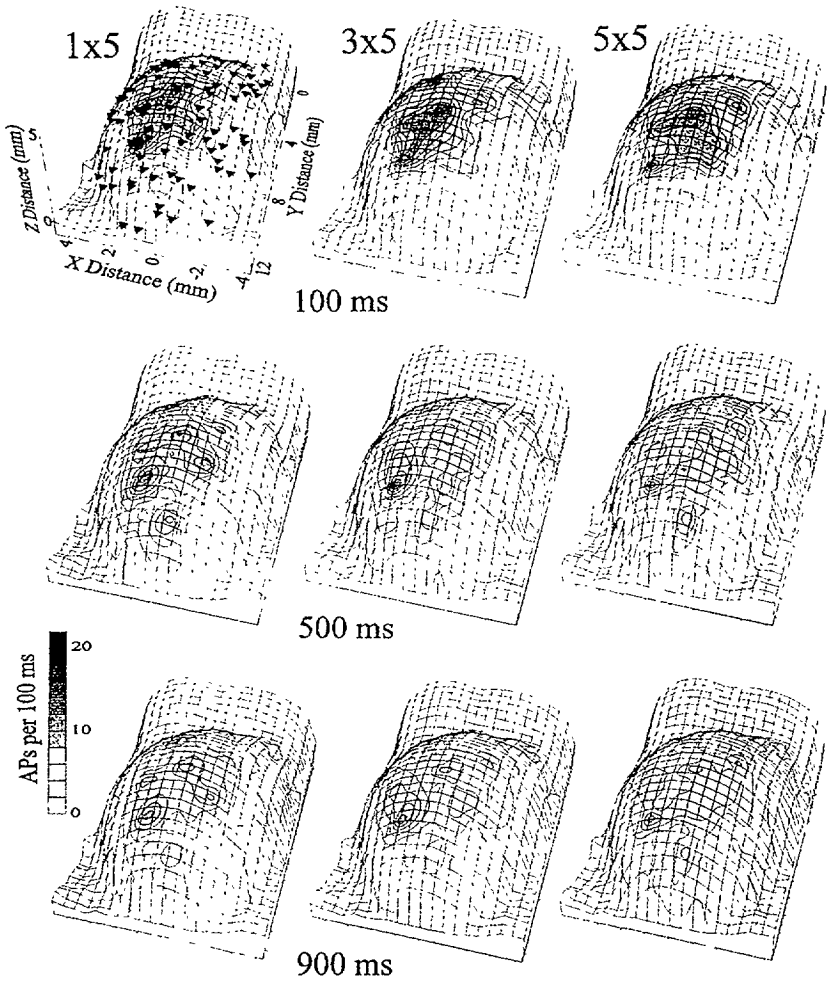

FIG. 4. SA population responses (PRs) to indentations at 90° orientation by the 3 objects at 100, 500, and 900 ms. Contour plots are superimposed on a geometric model of a monkey fingerpad. Magnitudes of the contours are the number of action potentials that occurred in a 100-ms time interval in response to the 1 × 5, 3 × 5 and 5 × 5 mm radii objects indented into the fingerpad. Small triangles on the *top left plot* indicate the locations of the most sensitive spots of the receptive fields of each afferent in the SA population. Color scale indicates the discharge rates.

spontaneously active; they only responded during the 4-s indentation. Typically, SAs responded to the indentation with a peak neural discharge occurring within the first 200 ms, which coincided with the fastest rate of compressional force (Fig. 3). The discharge rate then decreased exponentially reaching an equilibrium ("steady state") discharge rate at ~1 s after the initial skin contact. RAs reached heir peak discharge within the first 100 ms of the indentation; most did not respond at all after 400 ms. (Fig. 3). PCs responded only during the first 100 ms of the indentation (Fig. 3).

Mean von Frey thresholds for the SAs and RAs were 0.60 and 0.51 gwt, respectively (ranges: 0.035–5.10 gwt for both), and were not significantly different (one-way ANOVA, $P = 0.16$). There was no significant difference (two-way ANOVA) in the total number of action potentials for either the SAs or the RAs due to the different monkeys ($P = 0.08$), left or right hands ($P = 0.36$), or different fingers ($P = 0.65$).

Population encoding of shape

The SA PRs to indentation by the objects were nonisomorphic representations of the objects (Figs. 4 and 5). The PRs, represented by the 2D contour and 3D surface plots, were centered at the middle of the indentation site ($x = 0.0$ mm, $y = 8.3$ mm) and covered large areas of the fingerpad. The mound shaped appearance of the PRs was particularly evident in the surface plots. During the first 100 ms, the PRs to each of the indentations by the three objects were essentially the same whether viewing the 2D contour plots (Fig. 4) or the 3D surface plots (Fig. 5). At this time, there was little to distinguish the shapes of the SA PR_{Gf} (Fig. 6) or the parameters of those fits (Fig. 7). By 500 ms, clear differences in the 2D contours, 3D surfaces plots, and Gaussian surface fit parameters were present. By 900 ms, the PRs approached asymptotic values and were within 10% of the values they would achieve at 4 s.

Cross-sectional profiles, through the centers of the SA PRs along the minor axes, were also mound or Gaussian (2D) shaped (Figs. 8 and 9). These profiles were acquired from the PRs to indentations by objects oriented at 90° (major axis parallel to the long axis of the finger) and were centered close to the center of the indentation (or 0.0 m on the x axis). Over time, the central peaks of these profiles tended to drift toward the left (Fig. 8) such that during the last 3 s of the indentations, the average location of the central peaks was approximately offset 0.2 mm from 0. The center profiles qualitatively revealed three factors that were potentially important for encoding the shapes of the objects. First,

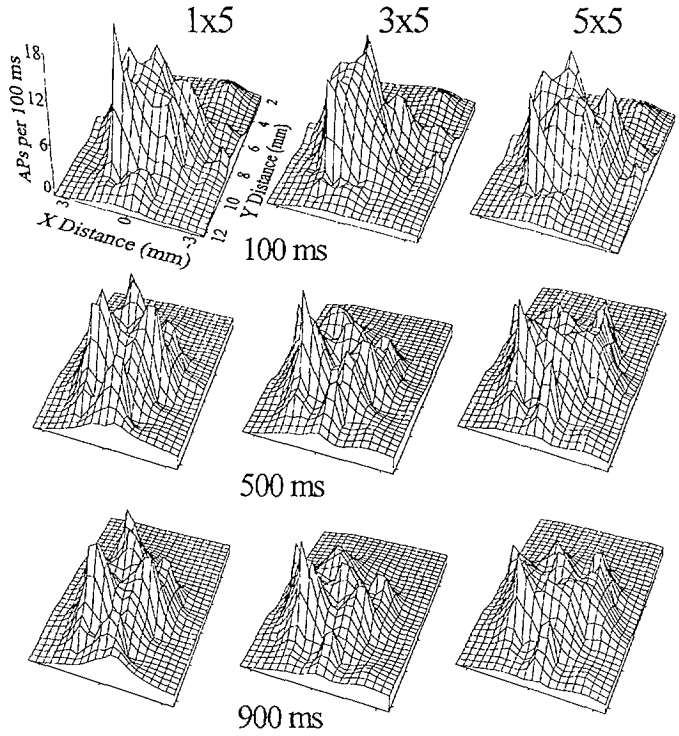

FIG. 5. SA PRs to indentations at 90° orientation by each object at 100, 500, and 900 ms, plotted as a 3-dimensional surface. Data were identical to those plotted as contours superimposed on the fingerpad in Fig. 4. z dimension is the number of action potentials that occurred during the designated 100-ms time intervals. Object radii were 1 × 5, 3 × 5, and 5 × 5 mm.

when normalized for peak discharge, the width, and overall shape of each profiles remained relatively constant after the first 300 ms of the indentation (Fig. 8). Second, once the PR had achieved relative equilibrium, during the last 3 s of the indentation, the width of the profile increased as the curvature of the minor axis of each object decreased (Fig. 9). And, third, also during equilibrium, the peak of the center profile increased as the minor axis curvature increased (Fig. 9). The overall similarity in the shapes of the PR profiles code for the similar circular nature of the cross-sectional profiles of the three objects. The differences in the parameters that characterize the PR shape (height, width, slopes) code the differences in the curvature of each object along the minor axes.

To quantitatively assess differences in the PRs that were related to differences in the shapes of the objects, three parameters of the PR_{Gf} were examined: peak discharge and the widths of the PR_{Gf} along the major and minor axes (Fig. 7). For all the objects, the peak discharge rate of the PR_{Gf} decreased at an exponential rate over time during adaptation of the PR. In general, for all the objects, the widths of the PR_{Gf} along the major and minor axes increased during the first 500 ms and thereafter maintained a constant value. These three parameters uniquely determined the shape of a Gaussian surface. The three objects all had identical curvatures of 200 m^{-1} (i.e., a radius of 5 mm) along the major axes. Correspondingly, the widths of the PR_{Gf} along the major axes (Fig. 7*C*) for the three objects over the 4-s indentation were not significantly different (ANOVA, $P > 0.05$). The widths of the PR_{Gf} along the minor axes (Fig. 7*B*) were significantly different (ANOVA, $P < 0.001$), as were the peak discharges (Fig.

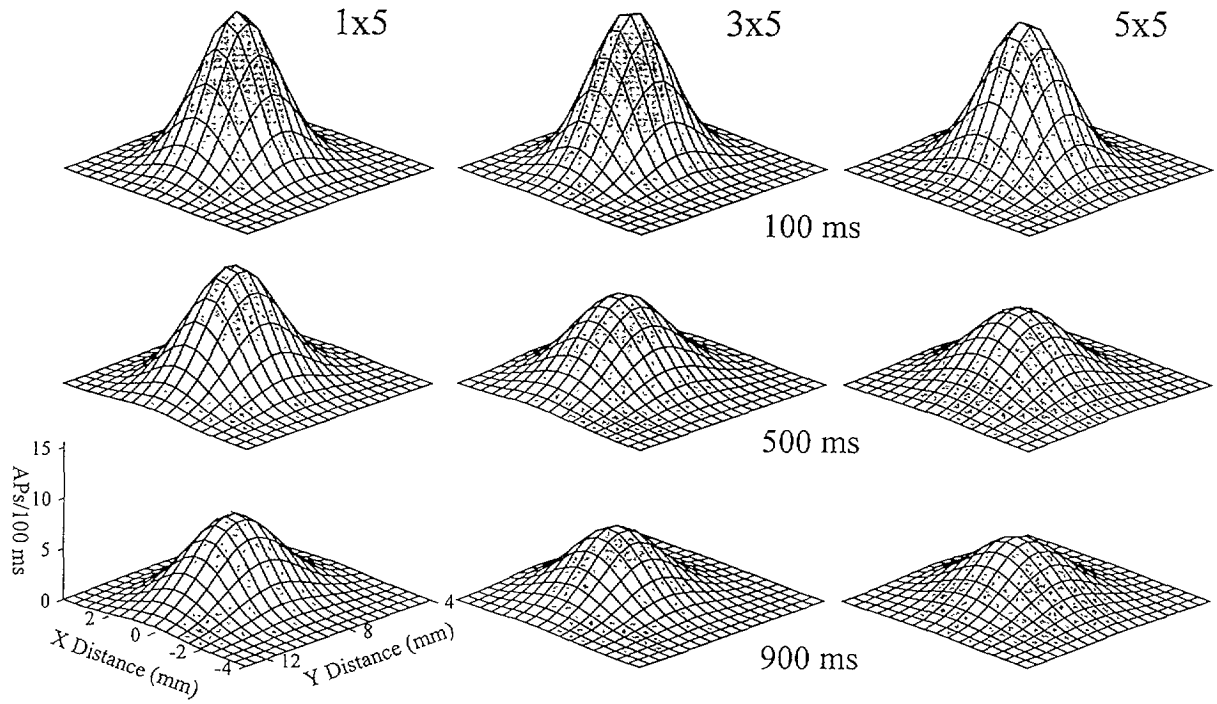

FIG. 6. Gaussian surface fits of the SA PRs to indentations at 90° orientation by each object at 100, 500, and 900 ms. Object radii were 1 × 5, 3 × 5, and 5 × 5 mm.

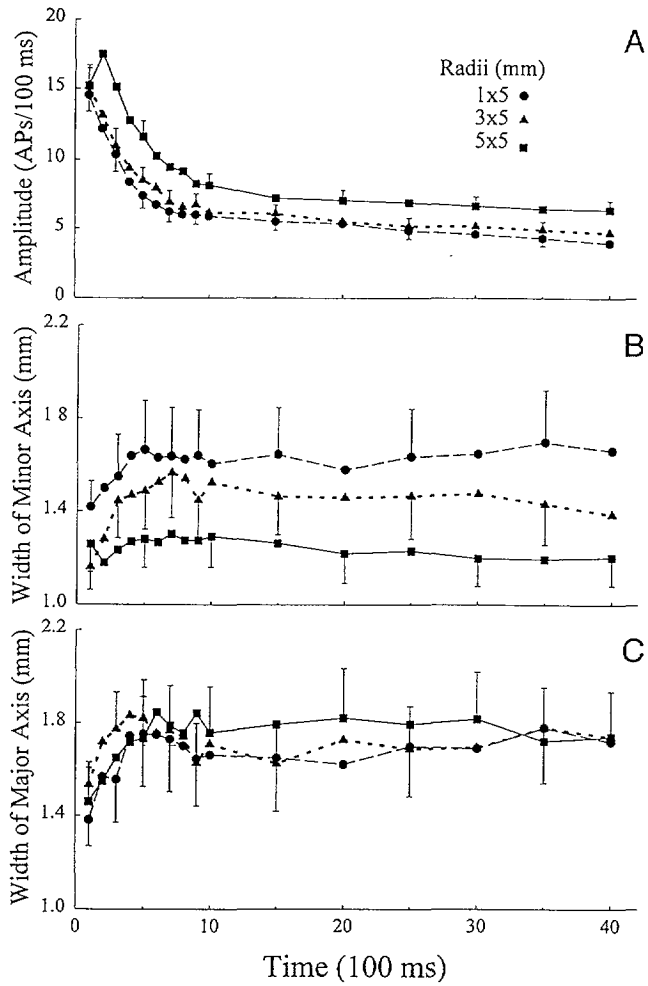

FIG. 7. Parameters of the Gaussian surface fits of the SA PRs at 90° orientation for each object during the 4-s Indentation. peak discharge (*A*) and the widths of the minor (*B*) and major (*C*) axes are the 3 parameters (*a*, *c*, and *e*, respectively, in the Gaussian equation) that uniquely determine the Gaussian surface. Error bars are standard errors of the means and are only shown for every other time period for figure clarity.

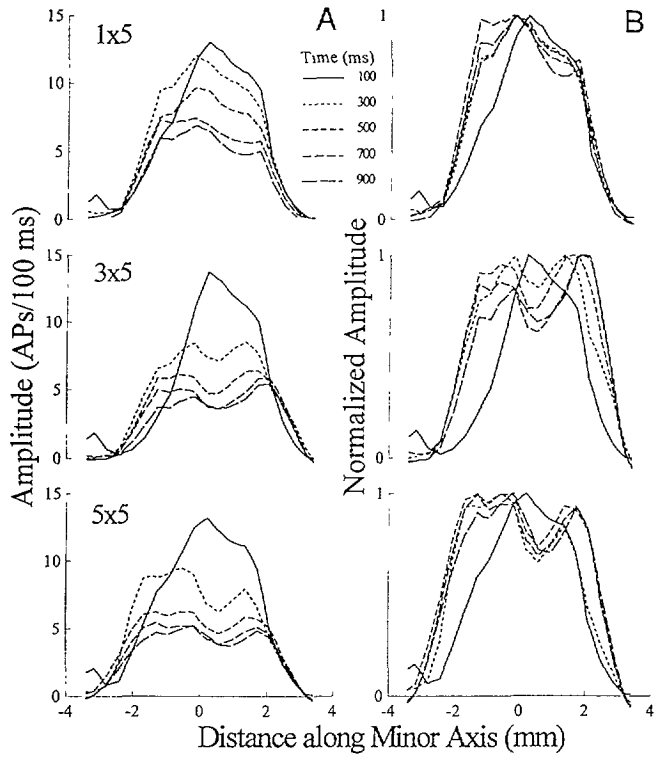

FIG. 8. Mean cross-sectional profiles through the SA PRs at discrete times. Profiles were obtained at the center of the indentation and parallel to the minor axis of the object with the object oriented at 90°. Amplitude of the response and number of action potential per 100 ms (APs/100 ms) are presented in absolute values (*A*) or normalized for peak discharge (*B*) at each time interval. Object radii were 1 × 5, 3 × 5, and 5 × 5 mm.

7*A*) of the surface fits (ANOVA, $P < 0.001$) over the 4-s indentation. The peak discharges were significantly different by 300 ms during indentation (two-way ANOVA, $P < 0.05$) and the widths of the PR_{Gf} along the minor axes by 400 ms (two-way ANOVA, $P < 0.05$). Thus the shapes of the PR_{Gf} remained significantly different from one another after the first 500 ms and were directly related to the differences in the curvatures of the actual objects.

The shapes of the SA PR_{Gf} were largely invariant with changes in orientation for each object (Fig. 10). The widths of the minor axes of the PR_{Gf} for different orientations were not significantly different (ANOVA, $P > 0.05$). The widths of the major axes were also not significantly different (ANOVA, $P > 0.05$), with the exception of the 3 × 5 at 45°. The peak discharges appeared to decrease slightly as the angle of orientation increased but the effect was not significant (ANOVA, $P > 0.05$).

The Gaussian surface fits were adequate representations of the PRs. The goodness of fit values were highest at the beginning of the indentation for each of the objects and orientations ($R^2 \sim 0.7$ during the first 100 ms) and decreased to a mean of 0.47 during the last 1 s of the indentation (Fig. 11). The orientation of the object did not significantly alter the goodness of fits. For the four orientations used in this study, the 1 × 5 mm object was fit better

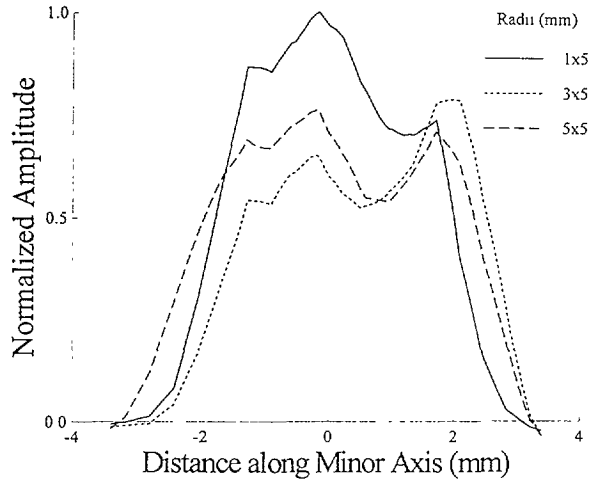

FIG. 9. Mean cross-sectional profiles through the SA PRs at 900 ms. Profiles obtained at the center of the indentation and parallel to the minor axis of the object with the object oriented at 90°. Neural discharge rates were normalized to the peak response that occurred in the PR at 900 ms to the 1 × 5 mm object. Object radii were 1 × 5, 3 × 5, and 5 × 5 mm.

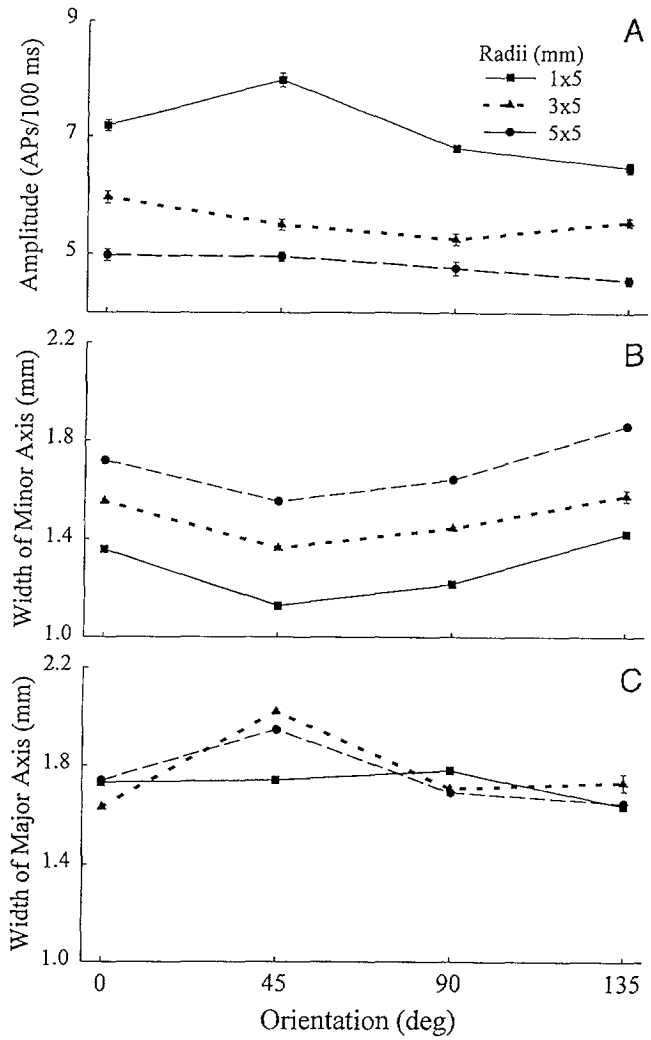

FIG. 10. Amplitude and width parameters from the Gaussian surface fits of the SA PRs averaged during the last 3 s of the indentation as a function of the angle of orientation of the object. Vertical axis were *A*: action potentials per 100 ms; *B*: width of the minor axis, and *C*: width of the major axis. Error bars are standard errors of the means and in many cases were too small to be seen on this scale.

by the Gaussian surface than the 3 × 5 or 5 × 5 (ANOVA, $P < 0.05$).

The contact widths and areas of the objects on the monkey fingerpad were compared with the area of the PR_{Gf} in the horizontal plane parallel to the surface of the skin and two orders of magnitude below the peak of the response. There were no significant differences in contact widths of the major axis for the three objects. In general, for the minor axis, the contact width increased as curvature decreased regardless of orientation; however, for the 3 × 5 mm object oriented at 0°, the contact width for the minor axis was comparable with the contact width for the major axis. For all orientations, contact area increased as the curvature of the objects decreased. During the last 3 of the 4 s of indentation, the area of the PR_{Gf} was always larger than the actual contact area for each of the three objects (Fig. 12). The horizontal extents of the PR_{Gf} for the three objects increased slightly with decreasing curvature of the minor axes. The PR_{Gf} extended beyond the boundaries of the actual contact regions by 1–1.9 mm.

The RA PRs did not adequately discriminate the shapes of the three objects. During the first 100 ms, the extent of their responses on the fingerpad was broader and the neural discharge of smaller magnitude (Figs. 13 and 14) than that for the SA PRs at the same time. By 300 ms, the RA PRs were substantially silent, whereas the SA PRs at 500 ms were still responding robustly. Most of the goodness-of-fit values (R^2) for the RA PR_{Gf} were <0.15. Because the R^2 values were so low, we deemed it inappropriate to compare the parameters of the surface fits.

We did not develop a spatial population response for the PCs because we encountered too few of them. Further, the response from the units we did record was completed within the first 100 ms. Given the inability of the RA PR to adequately discriminate between the shapes of the objects during the ~300-ms duration of their response, it appears highly unlikely that a PC population would have

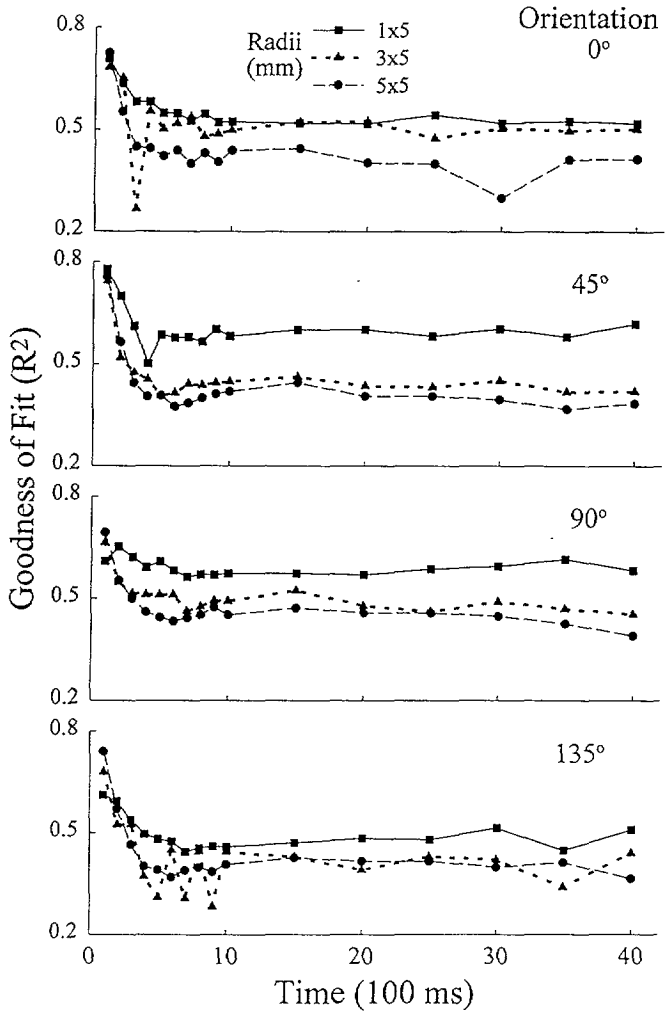

FIG. 11. Goodness-of-fit (R^2) of the Gaussian surfaces fits of the SA PRs at 0, 45, 90, and 135° orientations for the three objects during the 4-s indentation. Object radii were 1 × 5, 3 × 5, and 5 × 5 mm.

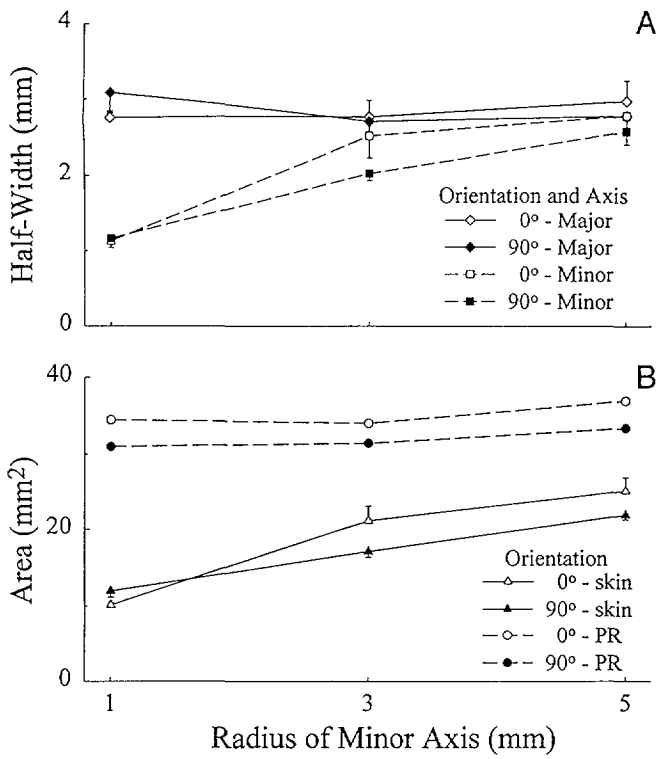

FIG. 12. Mean area and half-width measures of the contact area of each object on the skin and horizontal area of the SA PR. Each object was indented at orientations of 0 and 90° on the fingerpads of digits 2–4 of the left hand of a monkey. Widths and areas were obtained from imprints left from "inked" objects indented into the fingerpad with a force of 15 gwt for 4 s. *A*: mean half-widths of the major and minor axis of the object contact areas; *B*: mean object contact areas and area of the base of the Gaussian surface fits of the SA SPRs during the last second of the 4-s indentation. Error bars are standard errors.

any ability to encode shape during their shorter response duration of ~100 ms. However, they all responded to the indentations.

Population encoding of orientation

The physical orientations of each toroid (Fig. 15, *A* and *B*) were clearly distinguished by the orientations of the SA PR during the 4-s indentations (ANOVA, all $P < 0.001$). All pairwise comparisons of the PR orientations were significantly different from each other ($P < 0.05$). The four orientations of each toroid were discriminated within the first 300 ms. As expected, different "orientations" of the sphere (Fig. 15*C*) were not distinguished (ANOVA, $P = 0.32$). The orientation of the sphere was not random, but was strongly biased toward 90°, the long axis of the fingerpad. Orientation along 0° (transverse to the long axis of the fingerpad) as compared with the other three orientations was the least well fit for all the three objects as demonstrated by the higher standard errors of the mean in Table 1.

The orientations of the SA PRs to the toroids, averaged over time, showed a slight bias toward 90° but were linearly proportional to the physical orientations of the objects (Fig. 16). The slopes (0.76) and *y*-axis intercepts (~ 17°) of the regression lines were virtually the same for the toroids with high Pearson correlations ($R^2 = 0.97$ and 0.99, respectively). In contrast, the slope (0.12) and *y*-axis intercept (74°) of the regression line for the sphere was much different and had a relatively low Pearson correlation ($R^2 = 0.46$). Thus for different, asymmetrically shaped objects, the SA population consistently, and significantly, encoded their orientations.

Even though the RA PRs did not discriminate the shapes of the objects, they did roughly encode the orientations of the 1 × 5 (Fig. 17*A*) (ANOVA, $P = 0.006$) but not the 3 × 5 or 5 × 5 mm objects (Fig. 17, *B* and *C*; ANOVA, all $P > 0.1$) during the limited time they were responding. Both the 3 × 5 and 5 × 5 RA PRs were strongly biased toward ~45° for all the physical orientations of the objects. For the RA PR of the 1 × 5 mm object, all PR orientations were significantly different ($P < 0.05$) except for the 90 and 135° orientations. Further, the means of the 90 and 135° orientations for the 1 × 5 were confused by the RA PR (108 and 91°, respectively).

From the few PCs we recorded, we discerned no evidence that they would encode orientation.

DISCUSSION

The mechanoreceptor population responses were produced from afferents that were located on the fingerpads of digits 2–5, from both left and right hands and from five different monkeys. Undoubtedly, sampling afferents in this manner introduced some variance in our data that would not have been present had we had the capability of sampling an actual population of mechanoreceptors from a single fingerpad. However, we found no significant differences in the total responses of the afferents due to their being present on different fingers, different hands, or on different monkeys as has been similarly reported by others for monkeys (Goodwin et al. 1995) and cat and raccoon glabrous skin (Pubols 1982). Aside from the variability due to the differential sensitivity among fibers, the major source for the variance was probably caused by the differences in geometry and compliance of the different fingerpads (Srinivasan and Dandekar 1992). To minimize the effect of fingerpad geometry on our results, we selected monkeys with fingerpads that were similar in size. Although a monkey's finger is more flaccid than a humans, we maintained the monkeys hydration during the experiment in an attempt to minimize variations in flaccidity.

Another source of variation within the data were the alignment of the indenter to the same relative location on each fingerpad. Our analyses were predicated on indenting the center of each object, for every orientation, for each trial at the same relative location. Although this was done as accurately and consistently as possible, we estimate that the indentations occurred within a 0.25-mm radius of the desired location. This positional variability could have three effects. First, it could have slightly broadened the base area of the PR. Second, the positional variability would either increase or decrease the discharge rates of some units, increasing the "roughness" of the surface of the PR. And, third, it could have reduced the goodness-of-fit (R^2) of the PR_{Gf}.

We did not normalize the neural responses of afferents

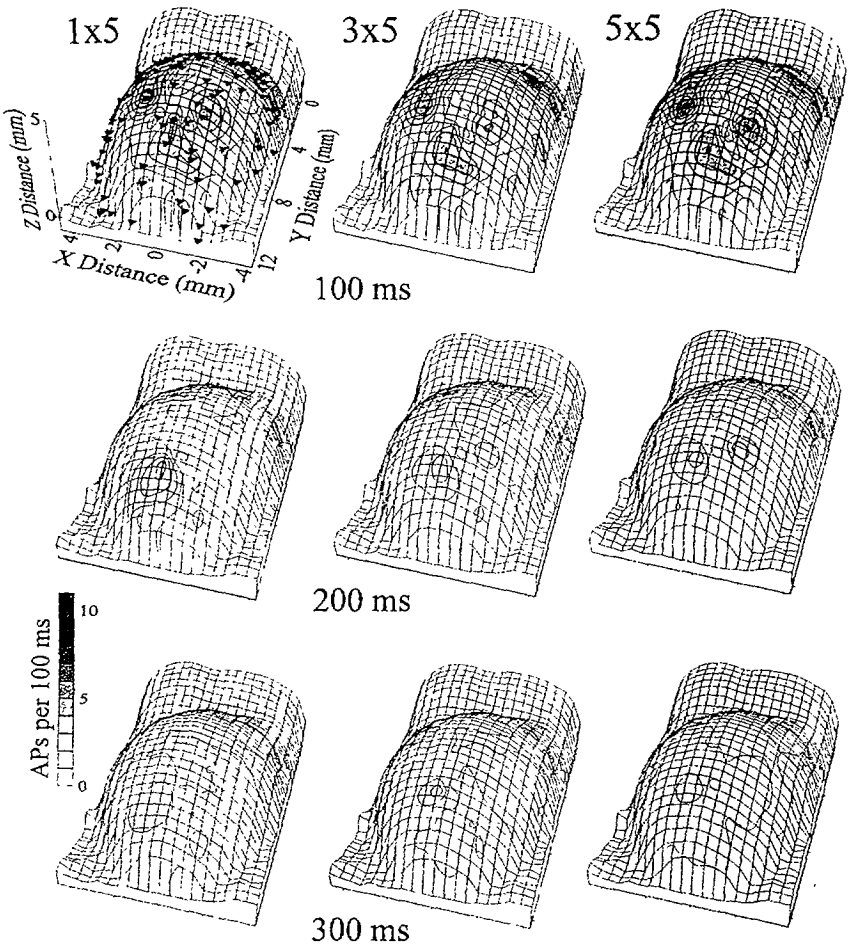

FIG. 13. RA PRs to indentations at 90° orientation by the three objects at 100, 200, and 300 ms. Contour plots are the same format as in Fig. 4. Small triangles on the *top left plot* indicate the locations of the most sensitive spot in the receptive field of each RA. Note the smaller magnitude scale and shorter time intervals used to depict the RA PRs in this figure vs. the SA PRs in Fig. 4.

for differences in their sensitivities to indentation. By using the raw data to depict the population response, we presented the peripheral neural representation before the first synapse in the CNS before central transformations. However, these raw data were susceptible to being skewed by the responses of a few very sensitive or very insensitive afferents. Afferents with thresholds that were >5.1 gwt were considered to be either high-threshold mechanoreceptors or actual nociceptors, and these units were eliminated from consideration. However, afferents with thresholds that were near but not greater this limit still had thresholds that were well over a magnitude greater than the least sensitive units. Sensitive units, on the other hand, had no lower limit. Two factors worked together to minimize the effects of sensitive and insensitive units. First, we obtained a population that approximated the actual number of units in a ~80 mm^2 area of a single fingerpad. Second, we fit that population with an equation for a Gaussian surface. The surface equation provided a robust means to represent the actual population because the inherent effects of sensitive and insensitive units would largely reduce the goodness-of-fit (R^2) and have minimal affects on the parameters which quantitatively described the PRs.

We chose to represent the neural response of the afferents to the indentations by binning their responses in 100-ms intervals, effectively a measure of instantaneous frequency. An alternative approach would be to accumulate their responses over time, invoking an aspect of neural memory. The cumulative approach would result in a larger absolute disparity between the peak responses of the PR_{GF} to the objects (Fig. 7). However, the percent differences between the peak responses at any given time during the 4-s indentation would generally be less than those calculated using the binned approach. Hence, discrimination between the shapes of the objects would tend to be better evaluated using smaller "windows" of time (sampling approach) rather than looking at it over longer periods of time (cumulative approach).

Shape encoding

The shapes of the objects indented into the monkey fingerpad were discriminated by the spatial population response. This discrimination was evident as early as 500 ms into the indentation in the SA PR_{Gf} and persisted for the rest of the 4-s duration. Although the RA population and the Pacinian afferents responded to the indentation, neither did so in a manner that demonstrated an ability to encode the shapes of the objects. Thus the ability of primates to perceive, by touch alone, the shapes of objects with curved surfaces develops solely from the SA PR. This finding is in

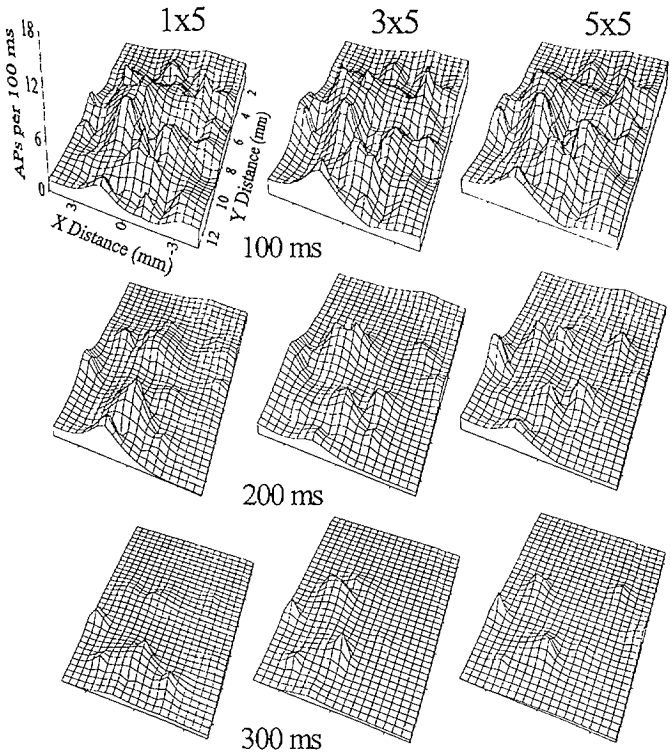

FIG. 14. RA PRs to indentations at 90° orientation by the three objects at 100, 200, and 300 ms plotted as a 3-dimensional surface. Data were the same as those shown as contours in Fig. 13. z dimension is the number of action potentials that occurred during 100-ms time intervals and has the same scale as that used for the SA PR in Fig. 5.

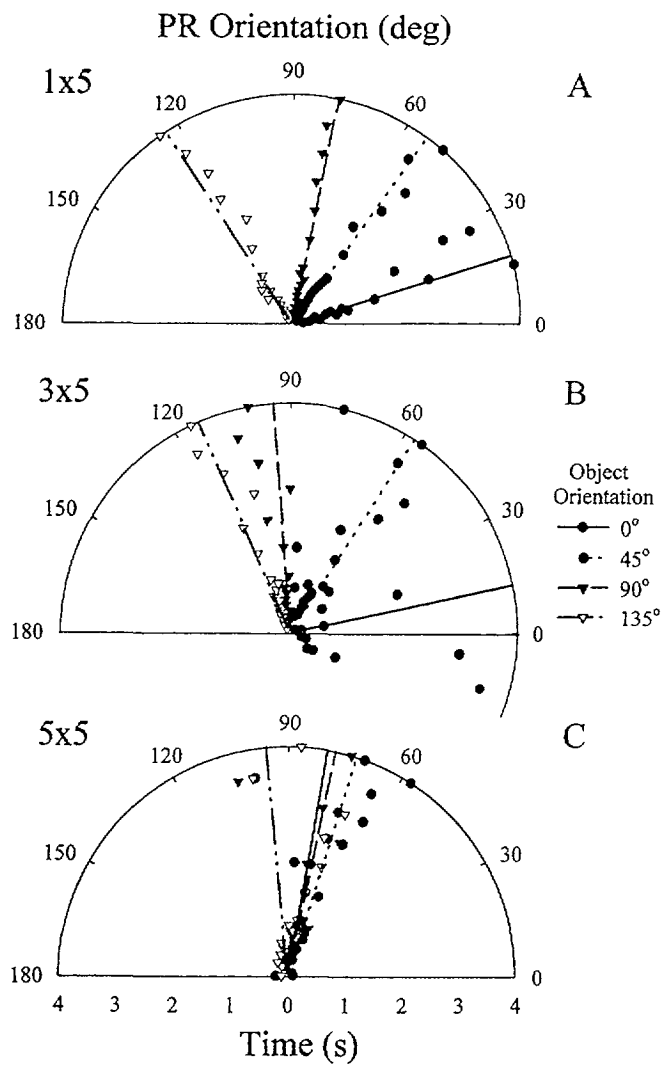

FIG. 15. Orientation encoding by the SA PRs for the three objects. In these polar plots, the radial axes are time (s) and the angular axes are orientation (deg). Symbols show the orientations of the PRs at individual 100-ms bins for each object and orientation, whereas the lines represent the mean angle of the major vector as determined by a weighted principal component analysis

agreement with results previously obtained from studies of shape coding in responses of individual afferents (Goodwin et al. 1995; Srinivasan and LaMotte 1987).

An important finding of this study was an explanation of how a noncompliant (i.e., hard) object would be perceived as maintaining its shape even though the responses of the peripheral afferents were changing. The shape of the SA PR remained constant after the initial contact period. That is, after the initial 500 ms of the indentation, the discharge rates of the individual afferents at different spatial locations remained proportional to each other even while their discharge rates were declining during adaptation. A proportional decline in discharge rate over time at different spatial locations also has been observed in SEP studies on single units (Cohen and Vierck 1993; Goodwin et al. 1995).

It has been hypothesized that when an object is stroked across the fingerpad, the distribution of the SA discharge rate encodes the distribution of curvatures of the object (LaMotte and Srinivasan 1996; LaMotte et al. 1996). This hypothesis was developed from observations of the spatial discharge profiles of single SAs and RAs. During a stroke, when the spatial response through the center of the RF was viewed in profile, the averaged slopes of the rising and falling phases of the response of the SAs, and not the RAs, were shown to be relatively constant and correlated with the constant curvature of the objects. Goodwin et al. (1995) found that indenting a sphere into the monkey fingerpad at higher forces simply results in a greater overall proportional population response. Similarly, indenting objects at the same force but at higher velocities results in a greater initial response (Cohen and Vierck 1993; Knibestol 1975), but after a steady state is reached in ~1 s, the population response will be the same. The current study extends these observations by

TABLE 1. *Standard errors of the means for orientation of population responses*

	Radii of Objects, mm		
Orientation, °	1 × 5	3 × 5	5 × 5
0	1.84	37.16	7 28
45	0.93	3.78	4.60
90	1 75	2 63	3.10
135	1.27	1.48	6.42

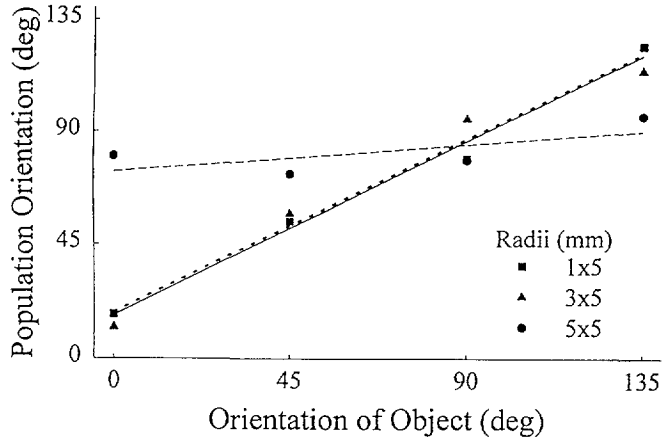

FIG. 16. Comparisons of the orientations of the SA PRs with those of the physical orientations of the objects. Symbols represent the average orientation over time for each of the objects. Lines represent the linear regression of the average orientations of the PRs for the 1 × 5 (——), 3 × 5 (· · ·), and 5 × 5 radii (mm) (– – –) objects.

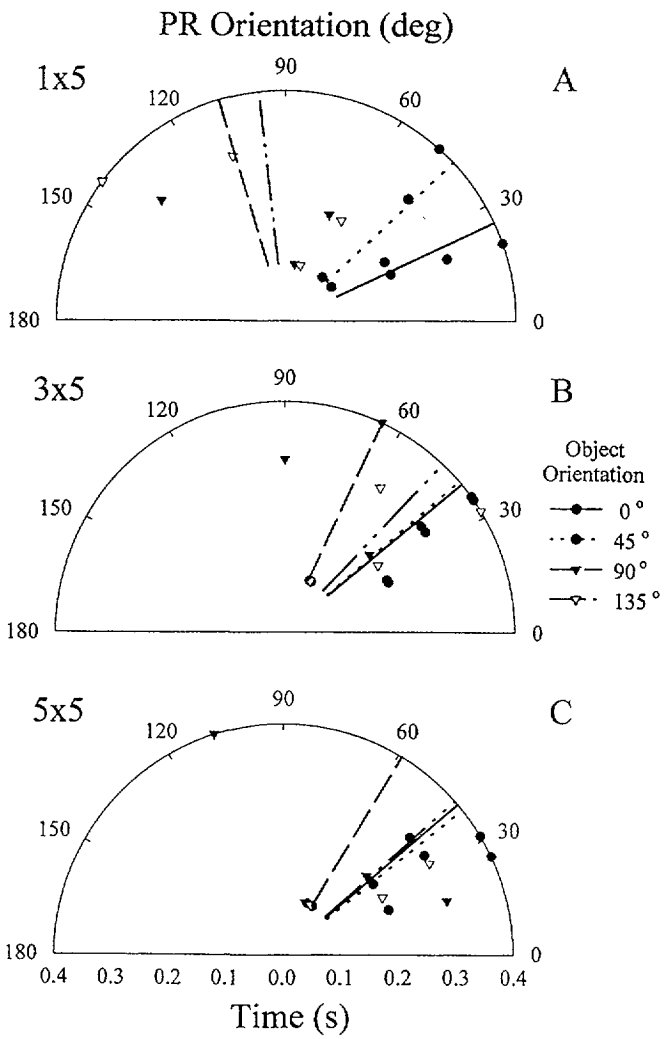

FIG. 17. Orientation encoding by the RA PRs for the 3 objects. Same format as in Fig. 15.

finding that the shape of the SA PR during indentation encodes the shape of asymmetrical objects.

Another important finding of this study was that the SA PRs discriminated the shapes and orientations of the objects without prior normalizing of the neural responses of the afferents for their substantial range of sensitivities. Previous studies (c.f., Goodwin et al. 1995) that estimated the response of a population to indentation have relied on normalizing for sensitivity, in part, because of the sparse number of units making up their database. One effect of normalizing our data would be, presumably, to improve the goodness-of-fit values of the Gaussian surfaces. However, in spite of the range in the sensitivities of individual SA afferents in our study, the nonnormalized SA PR credibly discriminated the shapes and orientations of the objects. Thus although it is conceivable that the CNS may in some fashion normalize the responses of individual afferents to account for different sensitivities, our data suggest that the normalization of the response of individual afferents may not be necessary to discriminate objects with sufficiently different shapes or orientations.

Qualitatively, our data compare favorably with those of Goodwin et al. (1995). They also found that the shape of a symmetrical object was well encoded by the spatial response of SAs but not by RAs nor PCs. Our Gaussian surface was similar to that of Goodwin et al. (1995): $z = f(x, y) = a \exp(-bx^2 - cy^2)$, except that we also included objects that were toroidal.

Using hemispherical indenters of different radii, Goodwin et al. (1995) found that the areal extent of the spatial response was only slightly larger as the radius of the indenter increased (or the curvature decreased). Thus as the radius of their hemispheres increased (or curvature decreased), the peak discharge of the SA afferents decreased and the extent of the afferents' response symmetrically broadened, though only slightly. Using toroidally shaped objects, we extended the findings of Goodwin et al. (1995) to show that the different widths of the minor axes were significantly discriminated by the PR_{Gf} even though the areal extents of the PR_{Gf}'s were only slightly different.

A previous investigation from this laboratory using spatial event plots (LaMotte et al. 1996) had predicted that the horizontal area of the base (i.e., the "footprint") of the PR would vary substantially depending on the size and shape of the indenting object. However, it has been demonstrated (Cohen and Vierck 1993; Goodwin et al. 1995) that individual SAs will respond to small magnitude indentations ≤3–4 mm away from the center of their receptive fields. Using finite element modeling of the monkey fingerpad to indentation, Srinivasan and Dandekar (1996) have estimated that significant mechanical stresses and/or strains develop ≤2.5 mm away from a simple line load. In our study, the areas of the bases of the PR_{Gf}, while being similar, were substantially larger than the contact area of the toroidal objects on the fingerpad. Thus even small objects, relative to the size of the fingerpad, broadly activate the cutaneous mechanoreceptor population on the fingerpad. Hence, it is primarily the spatial distribution of response intensities, rather than the extent of the population response on the fingerpad, that the nervous

system must use to determine the shape of an object during passive indentation.

Orientation encoding

Orientation encoding was primarily a function of the SA PR, although the RA PR provided limited information for objects of notable eccentricity during the dynamic phase of a stimulus. The RA PR weakly discriminated the orientations of the 1 × 5 but not the 3 × 5 or 5 × 5 mm objects. This difference in ability to encode orientation during indentation between the two types of populations (SAs vs. RAs) was primarily due to the lack of discharge by the RA PRs after 300 ms when the SA PRs were still discharging vigorously. The SA PRs only began to discriminate the different orientations ~300 ms into the indentation. This suggests that orientation discrimination would be poor if the duration of indentation is as short as 300 ms.

Using spatial event plots (SEPs), which estimate a population response from the responses of a single afferent stimulated by repeatedly stroking an object across its receptive field (RF) in parallel trajectories, RAs encoded orientation as well as SAs (LaMotte et al. 1996). However, there are notable differences between orientation encoding by a population of mechanoreceptors estimated by the SEP approach versus the approach used in the current study. First, stroking the object across the RF rather than indenting it into the fingerpad at a defined location is a much more effective stimulus for RAs. Although the magnitudes of the compressive force were equivalent, greater shear stress and shear strain were produced by stroking an object across rather than indenting it into the skin. Additionally, stroking produced both "ON" and "OFF" responses for the RAs as the object passed into and out of their RFs, whereas, the RAs only responded during the initial 300 ms during indentation. Second, although the objects used in the SEP study (LaMotte et al. 1996) had the same curvatures, they were much smaller in actual size. For a SEP to be an effective estimator of a PR for orientation (or shape) encoding, the object must be small enough so that it can enter into and exit from the RF. Smaller objects also produce smaller contact areas that would minimize the effects that the geometry of the fingerpad has on orientation (or shape) encoding.

Orientation encoding by the SA PR was notably influenced by the geometry of the fingerpad, with the orientation angle of the PR biased toward 90°, the long axis of the finger. Because the fingerpad is roughly cylindrical in shape, any axisymmetric object with dimensions on the same order of magnitude as the fingerpad itself (such as the toroidal objects we used) would develop different contact areas for different orientations. In particular, the fingerpad geometry would tend to increase the length of the contact area along the long axis of the fingerpad (Fearing and Binford 1991). This may account for the increases in the half-widths and areas observed (Fig. 12) and the very large variability in orientation encoding for the 3 × 5 mm object oriented at 0°.

In conclusion, shape and orientation encoding during static indentation appear to be functions of the spatially distributed SA population in the fingerpad.

We thank K. Greenquist and C Lu for technical assistance.

This work was funded by National Institutes of Health Grant 15888.

Address for reprint requests: R. H. LaMotte, Dept. of Anesthesiology, Yale University, 333 Cedar St., New Haven, CT 06510.

Received 8 October 1997; accepted in final form 23 February 1998.

REFERENCES

BURGESS, P. R., MEI, J., TUCKETT, R. P., HORCH, K. W., BALLINGER, C. M., AND POULOS, D. A The neural signal for skin indentation depth. I. Changing indentations. *J Neurosci.* 3: 1572–1585, 1983.

COHEN, R. H. AND VIERCK, C. J. Population estimates for responses of cutaneous mechanoreceptors to a vertically indenting probe on the glabrous skin of monkeys. *Exp. Brain Res.* 94: 105–119, 1993.

DANDEKAR, K. AND SRINIVASAN, M. A. A 3-dimensional finite element model of the monkey fingertip for predicting responses of slowly adapting mechanoreceptors. *Proc. ASME Bioeng, Conf.* 29. 257–258, 1995.

DARIAN-SMITH, I. AND KENNINS, P. Innervation density of mechanoreceptive fibers supplying glabrous skin of the monkey's index finger. *J. Physiol. (Lond.)* 309: 147–155, 1980.

DAVIS, J. C. *Statistics and Data Analysis in Geology*. New York: John Wiley, 1973.

FEARING, R. S. AND BINFORD, T. O. Using a cylindrical tactile sensor for determining curvature. *IEEE Trans. Robotics Autom.* 7: 806–817, 1991.

GOODWIN, A. W., BROWNING, A. S., AND WHEAT, H. E. Representation of curved surfaces in responses of mechanoreceptive afferent fibers innervating the monkey's fingerpad. *J. Neurosci.* 15: 798–810, 1995.

GOODWIN, A. W., JOHN, K. T., AND MARCEGLIA, A. H. Tactile discrimination of curvature by humans using only cutaneous information from the fingerpad. *Exp. Brain Res.* 86: 663–672, 1991.

GOODWIN, A. W. AND WHEAT, H. E. Human tactile discrimination of curvature when contact area with the skin remains constant. *Exp. Brain Res.* 88: 447–450, 1992a.

GOODWIN, A. W. AND WHEAT, H. E. Human tactile discrimination of curvature when contact area with the skin remains constant. *Somatosens. Mot. Res.* 9: 339–344, 1992b.

HULLIGER, M., NORDH, E., THELIN, A. E., AND VALLBO, A. B. The responses of afferent fibres from the glabrous skin of the hand during voluntary finger movements in man. *J. Physiol. (Lond.)* 291: 233–249, 1979.

KNIBESTOL, M. Stimulus-response functions of slowly adapting mechanoreceptors in the human glabrous skin area. *J. Physiol. (Lond.)* 245: 63–80, 1975.

LAMOTTE, R. H., LU, C., AND SRINIVASAN, M. A. Tactile neural codes for the shapes and orientations of objects. In: *Somesthesis and the Neurobiology of the Somatosensory Cortex*, ed. by O. Franzen, R. Johansson, and L. Terenius. Basel: Birkhäuser Verlag, 1996, pp. 113–122.

LAMOTTE, R. H. AND SRINIVASAN, M. A. Tactile discrimination of shape: responses of slowly adapting mechanoreceptor afferents to a step stroked across the monkey fingerpad. *J. Neurosci.* 7: 1655–1671, 1987.

LAMOTTE, R. H. AND SRINIVASAN, M. A. Neural encoding of shape: responses of cutaneous mechanoreceptors to a wavy surface stroke across the monkey fingerpad. *J. Neurophysiol.* 76: 3787–3797, 1996.

LAMOTTE, R. H., SRINIVASAN, M. A., AND KLUSCH-PETERSEN, A. Tactile discrimination and identification of the shapes and orientation of ellipsoidal objects. *Soc. Neurosci. Abstr.* 18: 830, 1992.

MEI, J., TUCKETT, R. P., POULOS, D. A., HORCH, K. W., WEI, J. Y., AND BURGESS, P. R. The neural signal for skin indentation depth. II. Steady indentations. *J. Neurosci.* 3: 2652–2659, 1983.

MORRISON, D. F. The structure of multivariate observations. I. Principal components. In: *Multivariate Statistical Methods* New York· McGraw-Hill, 1967, p. 266–299.

PHILLIPS, J. R. AND JOHNSON, K O. Tactile spatial resolution II. Neural representation of bars, edges, and gratings in monkey primary afferents. *J. Neurophysiol.* 46: 1177–1192, 1981.

POULOS, D. A., MEI, J., HORCH, K. W., TUCKETT, R. P., WEI, J. Y., CORNWALL, M. C., AND BURGESS, P. R The neural signal for the intensity of a tactile stimulus. *J. Neurosci.* 4: 2016–2024, 1984.

PUBOLS, B. H., JR. Factors affecting cutaneous mechanoreceptor response I. Constant-force versus constant-displacement stimulation *J. Neurophysiol.* 47: 515–529, 1982.

SRINIVASAN, M. A. Surface deflection of primate fingertip under line load *J. Biomech.* 22: 343–349, 1989.

SRINIVASAN, M. A. AND DANDEKAR, K. Role of fingertip geometry in the

transmission of tactile mechanical signals. In: *Advances in Bioengineering,* ed. M. W. Bidez, Bioengineering Division, vol. 22, p. 573–576, The American Society of Mechanical Engineers, 1992.

SRINIVASAN, M. A. AND DANDEKAR, K. An investigation of the mechanics of tactile sense using two-dimensional models of the primate fingertip. *J. Biomech. Eng.* 118: 48–55, 1996.

SRINIVASAN, M. A. AND LAMOTTE, R. H. Tactile discrimination of shape: responses of slowly and rapidly adapting mechanoreceptive afferents to a step indented into the monkey fingerpad. *J. Neurosci.* 7: 1682–1697, 1987.

SRINIVASAN, M. A. AND LAMOTTE, R. H. Encoding of shape in the responses of cutaneous mechanoreceptors. In: *Information Processing in the Somatosensory System*, edited by O. Franzen and J. Westman. London: MacMillan, 1991, p. 59–69.

SRINIVASAN, M. A., WHITEHOUSE, J. M , AND LAMOTTE, R. H. Tactile detection of slip: surface microgeometry and peripheral neural codes. *J. Neurophysiol.* 63: 1323–1332, 1990.

WHEAT, H. E., GOODWIN, A. W., AND BROWINING, A. S. Tactile resolution: peripheral neural mechanisms underlying the human capacity to determine positions of objects contacting the fingerpad. *J. Neurosci.* 15: 5582–5595, 1995.